crystals

MDPI

Review

Electrocatalytic NO Reduction to NH_3: Theoretical Advances in Low-Dimensional Materials, Interfaces, and Microenvironments

Yu Liang [1], Daoming Zhang [1], Weiyi Wang [2,*], Shijie Xiong [3,*], Hua Yang [1] and Jiajun Wang [1,*]

[1] Tianjin Key Laboratory of Structure and Performance for Functional Molecules, College of Chemistry, Tianjin Normal University, Tianjin 300387, China; tjnuly@stu.tjnu.edu.cn (Y.L.); zhangdaoming9068@163.com (D.Z.); hxxyyh@tjnu.edu.cn (H.Y.)
[2] Hefei National Research Center for Physical Sciences at the Microscale & State Key Laboratory of Precision and Intelligent Chemistry, University of Science and Technology of China, Hefei 230026, China
[3] Beijing National Laboratory for Molecular Sciences & College of Chemistry and Molecular Engineering, Peking University, Beijing 100871, China
* Correspondence: dancingw@ustc.edu.cn (W.W.); 1701110353@pku.edu.cn (S.X.); hxxywjj@tjnu.edu.cn (J.W.)

Abstract

Electrocatalytic nitric oxide reduction reaction (NORR) for ammonia synthesis has emerged as a research focus in artificial nitrogen fixation. Unlike previous reviews that primarily focus on experimental catalyst development , this work offers a comprehensive and systematic summary of recent theoretical progress in NORR, with special emphasis on low-dimensional materials. We connect four important areas: atomic-level design principles for active sites, emerging mechanistic ideas that go beyond conventional scaling relations, realistic simulations of the electrochemical microenvironment, and data-driven machine learning approaches for catalyst discovery. We begin by discussing the reaction mechanism, analyzing the orbital interactions that control NO activation and the thermodynamic and kinetic features of different reaction pathways. For active-site construction, we examine electronic synergy in single-atom and dual-atom catalysts, coordination microenvironment tuning, electronic structure modulation through doping and strain, and heterojunction interfaces that allow multi-degree-of-freedom regulation. To explore new mechanistic concepts, we introduce *p*-block element synergy, reverse activation, magnetic and spin control, and surface electronic singularities as strategies to overcome traditional scaling relations. Regarding the reaction microenvironment, we analyze how coverage, solvation, local pH, and applied potential jointly affect selectivity and activity. Finally, we summarize the role of machine learning in building descriptors and accelerating catalyst screening. This review aims to provide theoretical guidance for the rational design of efficient NORR electrocatalysts with high activity, selectivity, and long-term stability.

Keywords: electrocatalytic nitric oxide reduction; ammonia synthesis; active site engineering; electronic structure regulation; reaction microenvironment; machine learning

Check for updates

Academic Editor: Jan Macutkevic

Received: 8 April 2026
Revised: 30 June 2026
Accepted: 1 July 2026
Published: 7 July 2026

Copyright: © 2026 by the authors. Licensee MDPI, Basel, Switzerland. This article is an open access article distributed under the terms and conditions of the Creative Commons Attribution (CC BY) license.

1. Introduction

Nitric oxide (NO) is a byproduct of fossil fuel combustion, industrial emissions, and biological metabolism. It is also a significant atmospheric pollutant that causes acid rain, photochemical smog, and stratospheric ozone depletion. Conventional denitrification technologies, such as selective catalytic reduction (SCR), effectively remove NO. However, they typically require high temperatures, precious metal catalysts, or additional reducing agents [1,2]. These processes are energy-intensive, often generate secondary pollution, and

fail to convert NO into value-added products. With the rapid development of renewable energy technologies, the direct conversion of NO into chemicals such as ammonia (NH_3) under mild conditions has attracted research interest. This interest lies at the nexus of energy catalysis and environmental science. Driven by renewable electricity, the electrocatalytic nitric oxide reduction reaction (NORR) converts NO to NH_3 at ambient temperature and pressure. This process offers the dual benefits of pollutant mitigation and green NH_3 synthesis [3–5]. NORR has distinct thermodynamic and kinetic advantages over the electrocatalytic nitrogen reduction reaction (NRR). For example, the N–O bond energy (607 kJ/mol) is much lower than that of N≡N (941 kJ/mol). NO also has higher aqueous solubility. Moreover, its standard potential (+0.71 V vs. RHE) is more positive than that of the competing hydrogen evolution reaction (HER, 0.00 V). This positive potential inherently suppresses side reactions. Consequently, NORR is seen as a viable pathway for "waste-to-wealth" conversion and helps close a clean artificial nitrogen cycle.

Low-dimensional materials offer several distinct advantages for NORR compared to conventional bulk catalysts. Representative low-dimensional catalytic systems include single-atom catalysts (SACs) [6–10], dual-atom catalysts (DACs) [11–14], and two-dimensional (2D) materials such as carbon-based materials [15–18], transition metal dichalcogenides (TMDs) [19–23], and MXenes [24–26]. First, their high surface-to-volume ratios maximize active-site exposure, enabling efficient utilization of catalytic metals. Second, the precisely tunable coordination environments in SACs and DACs allow fine control over the electronic structure of active centers. Third, the confinement effects inherent to low-dimensional structures can suppress undesired side reactions, such as N-N coupling and hydrogen evolution. Fourth, researchers can continuously modulate the catalytic properties of 2D materials through strain engineering, doping, and heterojunction construction. These features make low-dimensional materials highly attractive as platforms for NORR catalyst design.

However, practical NORR systems face multiple challenges. The paramagnetic nature of NO leads to diverse adsorption configurations (e.g., N-end-on, O-end-on, side-on) on catalyst surfaces, creating complex reaction networks [27,28]. The evolution pathways of intermediates (*NO, *NOH, *N, *NH) depend strongly on the atomic arrangement and electronic structure of catalytic centers. Simultaneously, the competitive HER consumes electrons and protons, limiting the Faradaic efficiency toward NH_3. Additionally, strong NO adsorption can poison active sites [29]. Furthermore, the solid–liquid interface has local pH gradients, electric field distributions, and solvation networks. These factors make it difficult for static density functional theory (DFT) calculations to accurately describe dynamic reaction processes, creating a gap between theoretical predictions and experimental observations. Bridging this gap requires operando characterization techniques, such as in situ X-ray absorption spectroscopy (XAS), environmental transmission electron microscopy (ETEM), and surface-enhanced infrared absorption spectroscopy (SEIRAS). Such techniques can track the dynamic evolution of active centers under realistic reaction conditions.

Against this background, we focus on the application of low-dimensional materials in NORR. Our review differs from previous ones that primarily focus on experimental catalyst development. It provides a systematic integration of recent theoretical advances. We connect active-site design principles, emerging mechanistic concepts beyond scaling relations, realistic microenvironmental simulations, and machine learning approaches. Starting from reaction mechanisms, this review systematically summarizes research progress across five areas: active-site construction, electronic structure regulation, exploration of new mechanisms, microenvironmental effects, and machine learning applications. The aim is to synthesize existing theoretical achievements and identify key challenges. It also

aims to provide a systematic reference for the design and application of high-performance NORR electrocatalysts.

2. Reaction Mechanisms and Performance Metrics

The electrocatalytic NO-to-NH_3 conversion involves a complex network requiring the transfer of five proton–electron (H^+/e^-) pairs. On transition metal surfaces, the activation mechanism follows a "donation/back-donation" model of bidirectional charge transfer. Specifically, the d-orbitals of surface metal sites overlap with the σ-bonding orbital of NO; NO donates electrons from its σ-orbital into the empty d-orbitals of the metal, while simultaneously, occupied metal d-orbitals back-donate electrons into the empty π^* orbital of NO. This orbital hybridization weakens the N-O bond, elongates the bond length, and constitutes the initial activation step. Based on the timing of N-O bond cleavage, NORR pathways are broadly classified into dissociative and associative mechanisms. Under mild electrocatalytic conditions, the associative mechanism dominates. Depending on the hydrogenation sequence and initial adsorption geometry, the associative mechanism can be further divided into alternating and distal pathways (Figure 1):

(1) Alternating pathway (N-end initiated): protons alternately attack the N and O atoms, proceeding via *HNO → *HNOH → *H_2NOH → *NH_2, ultimately yielding NH_3.
(2) Alternating pathway (O-end initiated): protons preferentially attack the O atom to form *NOH, followed by *HNOH → *NH → *NH_2 to produce NH_3.
(3) Distal pathway: protons continuously attack the atom (either N or O) farther from the metal surface until it desorbs as H_2O or NH_3. Subsequently, the remaining atom adsorbed directly on the surface is hydrogenated.

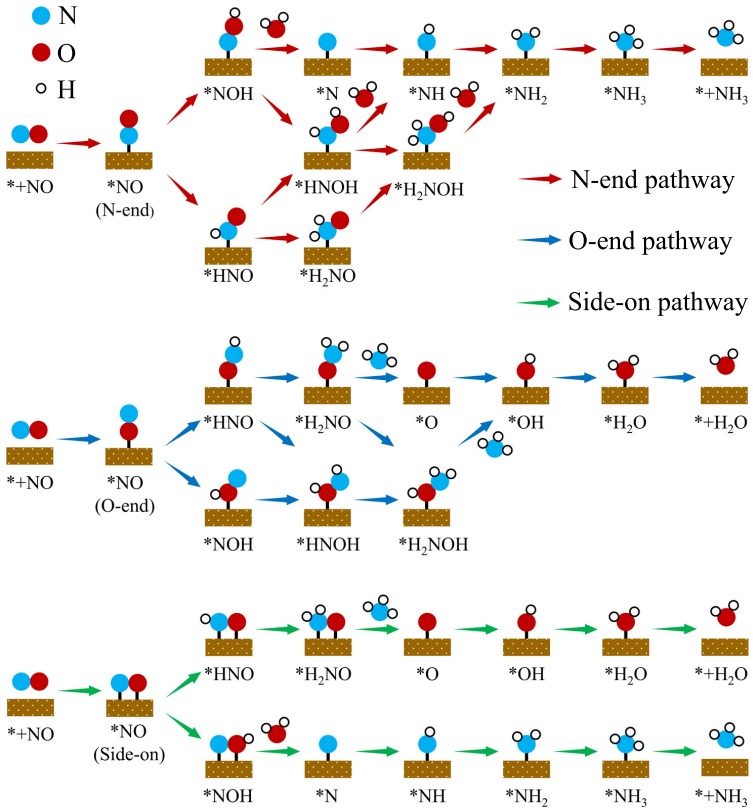


Figure 1. Schematic illustration of possible pathways for electrocatalytic NORR to NH_3.

The potential-determining step (PDS) in NORR varies with the geometric and electronic structure of the catalyst, typically occurring either during the initial hydrogenation of

NO to form *NHO/*NOH or during the later-stage hydrogenation of $*NH_2$. Moreover, under conditions of high NO concentration and high surface coverage, adjacent *NO species can couple to form an $*N_2O_2$ dimer intermediate. This diverts the reaction from the desired ammonia pathway toward byproducts such as N_2O and N_2, representing a major challenge in controlling NORR selectivity.

Assessing catalytic performance in NORR requires a multi-dimensional evaluation framework grounded in three core metrics: activity, selectivity, and stability. Quantitative structure–function relationships are typically established through activity descriptors that link atomic-scale crystallographic features to macroscopic catalytic behavior. From a thermodynamic perspective, the limiting potential (U_L) and overpotential derived from the computational hydrogen electrode (CHE) model are key metrics. U_L is determined by the maximum free energy change in the PDS ($U_L = -\Delta G_{max}/e$). Efficient catalysts should exhibit low U_L and overpotential to minimize the energy input required. Kinetically and in terms of selectivity, Faradaic efficiency and NH_3 selectivity are critical benchmarks. Suppressing the competing HER and undesired N-N coupling requires both a significantly more positive U_L for NORR relative to HER and kinetic suppression of $*N_2O_2$ intermediate formation. Stability assessment encompasses chemical stability, lattice structural integrity, and electrochemical durability, often evaluated via ab initio molecular dynamics (AIMD) simulations. Practical catalysts must exhibit robust resistance to metal dissolution, nanoparticle agglomeration, and surface passivation under realistic operating conditions. Collectively, these performance metrics establish a quantitative foundation for the rational design of catalysts that concurrently optimize activity, selectivity, and durability.

3. Active-Site Engineering and Surface/Interface Design

The rational design of highly active and selective NORR electrocatalysts critically depends on the precise engineering of active sites at the atomic level. Current research has evolved into a multifaceted framework that integrates six core strategies: SACs, DACs, coordination microenvironment engineering, heteroatom doping, strain engineering, and heterojunction construction. These approaches enable the fine-tuning of both the geometric configuration and electronic structure of active centers. The overarching goal is to overcome the inherent limitations of conventional catalysts by optimizing the adsorption strength of NO and its intermediates, thereby steering the reaction pathway toward efficient NH_3 production while suppressing the competing HER.

3.1. Single-Atom Catalysts

SACs, characterized by maximum atom utilization, uniformly distributed active sites, and a well-defined coordination environment, provide an ideal platform for unraveling NORR mechanisms and developing efficient catalysts [30,31]. The catalytic performance of SACs is critically dependent on the ability of the support to modulate the *d*-orbital electronic structure of the isolated metal center. Recent theoretical studies on various 2D supports have established that tailoring the support's electronic properties and defect chemistry can align the metal d-orbitals with the antibonding orbitals of NO, promoting activation while disfavoring HER. For instance, Wang et al. [32] systematically evaluated a series of TMN_4 moieties (TM = V, Cr, Mn, Fe, Co, Ni, Cu, Ru, Rh, Ta) and identified FeN_4 as a promising candidate, exhibiting a moderate NO adsorption energy (−2.04 eV) and a low energy barrier of 0.58 eV for the PDS (*NO → *NOH). Through crystal orbital Hamilton population (COHP) analysis, they established a linear relationship between the free energy of adsorbed nitrogen (ΔG_{ads}(*N)) and the TM-N bond strength, offering a valuable descriptor for catalyst screening. Expanding the support library, Jacob et al. [23] demonstrated that a single Cu atom anchored on a WS_2 monolayer facilitates the N-alternating pathway (*NO → *HNO

$\rightarrow$ *NH_2OH $\rightarrow$ *NH_2 $\rightarrow$ *NH_3), with the hydrogenation of *NH_2OH to *NH_2 being the PDS (0.41 eV). Bader charge analysis confirmed that significant electron transfer (0.24 e^-) from the substrate to NO elongates and activates the N-O bond. Duan et al. [33] identified V@VS_2 as a highly active site with an ultralow U_L of -0.20 V, further confirmed by AIMD simulations demonstrating its robust stability at 500 K. Furthermore, Kong et al. [34] highlighted the critical issue of single-atom stability, showing that the aggregation of Cu or Ni atoms on $Ti_3C_2T_x$ into clusters drastically alters the electronic structure. The increased density of states near the Fermi level in these clusters leads to overbinding of intermediates and even shifts the product selectivity towards N_2O in the case of Ni clusters, underscoring the necessity of maintaining atomic dispersion.

The search for optimal SACs has also extended to novel metal centers. Yan et al. [15] expanded the horizon to rare-earth metals and found that a LaN_4 moiety in graphene, owing to its unique *4f* electronic structure, promotes significant charge transfer to NO (0.71 e^-). This makes the first hydrogenation step (*NO $\rightarrow$ *HNO) exceptionally favorable, outperforming traditional transition metal centers. These collective efforts underscore that key descriptors such as the *d*-band center, charge transfer capability, and adsorption free energies of intermediates govern NORR activity, thereby laying a solid theoretical foundation for the rational design of high-performance SACs.

3.2. Dual-Atom Catalysts

Despite the successes of SACs, their activity is often constrained by the linear scaling relationships that couple the adsorption energies of different intermediates. DACs have emerged as a powerful strategy to circumvent this limitation [35–37]. The synergistic interaction between two proximal metal atoms provides an additional degree of freedom, enabling the independent modulation of adsorption energies for different intermediates and providing a structural basis for breaking traditional scaling relations [38].

Systematic theoretical screenings have been instrumental in identifying promising DAC candidates. As shown in Figure 2, Sun et al. [39] screened 78 transition metal dimers supported on *g*-CN (TM_1TM_2@*g*-CN) for the NORR. Through a five-step high-throughput screening strategy, they identified TiCr@*g*-CN (-0.37 V), TiMo@*g*-CN (-0.36 V), and MnMo@*g*-CN (-0.43 V) as promising catalysts with low overpotentials. Notably, MoMo@*g*-CN was found to spontaneously reduce NO without any thermodynamic energy barrier, which was attributed to the synergistic electronic modulation between adjacent Mo atoms that optimizes intermediate adsorption. Zang and co-workers [40] screened 24 transition metal dimers supported on C_2N, identifying Cr_2@C_2N as a highly stable and active system. They established a volcanic relationship between activity and adsorption energies of N atom (ΔE_{*N}) and NO molecule (ΔG_{*NO}), providing a simple yet effective descriptor for DAC design. Fan et al. [41] expanded the search space to 784 heteronuclear combinations on N-doped graphene (TM_1TM_2/N-G) and, through a four-step screening strategy, pinpointed CuAg/N-G with an exceptionally low U_L of 0.07 V. Projected density of states (PDOS) and COHP analyses revealed the synergistic electronic regulation between Cu and Ag during NO activation, with Cu and Ag playing complementary roles in the first and last hydrogenation steps.

Furthermore, DACs offer a platform for fine-tuning product selectivity. Zhu and co-workers [14] introduced axial O ligands to modulate the electronic structure of phthalocyanine-based M_2-Pc dimers. This modification significantly reduced the energy barriers for O-Ni_2-Pc and O-Cu_2-Pc. In contrast, systems like Co_2-Pc and Cr_2-Pc were found to promote N-N coupling under high NO coverage, leading to N_2O formation. This study highlights NO adsorption energy (ΔE_{*NO}) as an effective descriptor for predicting and controlling product selectivity in DACs. Zhao et al. [42] demonstrated that the het-

eronuclear Fe-Cu pair on nitrogen-doped graphene (FeCu/N-G) can directly reduce NO to N_2 via the Langmuir–Hinshelwood mechanism, where electron transfer between Fe and Cu is the key to enhanced activity. Therefore, it can be anticipated that, with ongoing advances in the precise structural engineering and controllable synthesis of DACs, this strategy will assume an increasingly pivotal role in NORR.

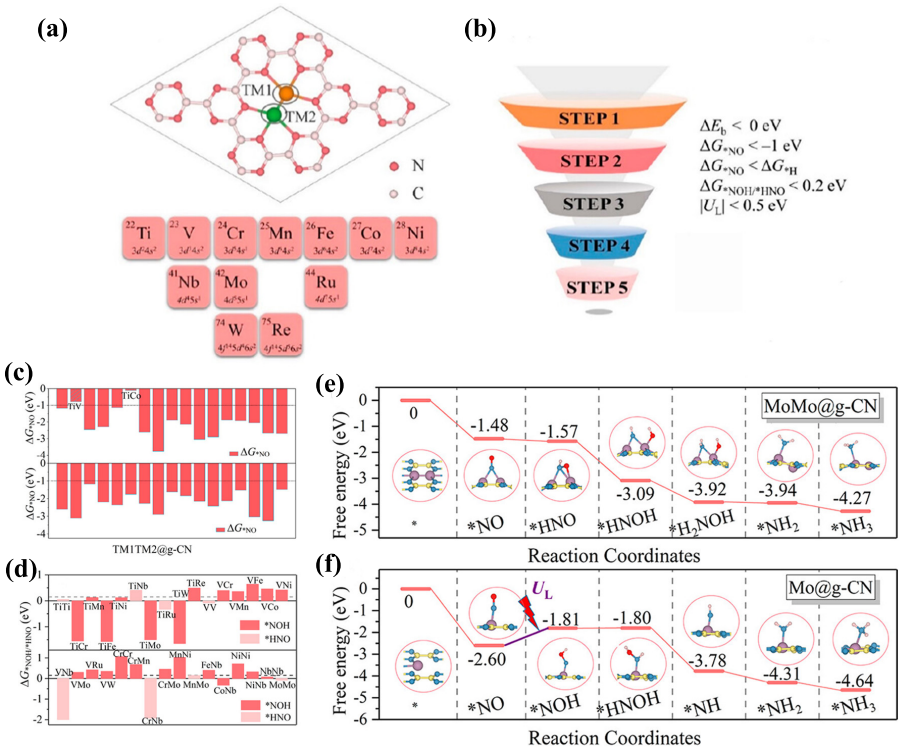


Figure 2. (**a**) Top view of the TM_1TM_2@*g*-CN structure illustrating the range of transition metals considered for dual-atom catalysts. (**b**) Five-step screening strategy for identifying promising NORR electrocatalysts. (**c**) Calculated ΔG_{*NO} values for the most stable NO adsorption configuration on 34 stable DAC candidates. (**d**) Preferred intermediate after the first hydrogenation step (*NOH or *HNO) and corresponding ΔG values for 32 TM_1TM_2@*g*-CN systems. Gibbs free energy diagrams for NORR on (**e**) MoMo@*g*-CN and (**f**) Mo@*g*-CN along the optimal reaction pathway, with corresponding optimized intermediate structures shown. Reproduced from Ref. [39] with permission from the American Chemical Society.

3.3. Coordination Microenvironment Engineering

Beyond the choice of metal center, fine-tuning the local coordination environment has become a cornerstone for optimizing NORR performance. This involves manipulating the number, type, and spatial arrangement of ligands around the active site. Li et al. [43] systematically constructed 26 Fe-based SACs with different coordination configurations and discovered that pyrrole-type FeN_4 and pyridine-type FeN_3O possess extremely low limiting potentials (−0.26 V and −0.33 V, respectively). Through electronic structure analysis, they elucidated the electron "donation/back-donation" activation mechanism on the Fe center. In this process, the Fe *d*-orbitals back-donate electrons to the NO π^* orbitals and simultaneously accept the σ lone-pair electrons from NO, thereby achieving efficient activation. Furthermore, the *d*-band center of Fe exhibits a good linear correlation with NORR activity ($R^2 = 0.85$), serving as an effective descriptor for predicting catalytic performance.

Extending this concept to the second coordination sphere, Zhu et al. [44] employed a constant-potential/hybrid-solvent model combined with microkinetic simulations to investigate the effects of doping O or B atoms in the second coordination sphere on the

NORR performance of FeN_4 catalysts. They found that the introduction of O or B atoms modulates the *d*-band center of the Fe site, thereby altering the adsorption strength of reaction intermediates: the high electronegativity of the O atom shifts the *d*-band center downward, weakening adsorption, while the electron-deficient nature of the B atom shifts the *d*-band center upward, strengthening adsorption. Among the studied catalysts, the pristine FeN_4 catalyst achieved NH_3 production at −0.70 V vs. RHE, exhibiting the lowest overpotential and optimal catalytic activity, whereas O or B doping led to increased reaction barriers and decreased activity.

Axial coordination offers another powerful handle. Sun et al. [45] explored the impact of axial ligands (e.g., O, F, Cl) on TMN_4-C model catalysts (Figure 3). They found that these electron-withdrawing axial atoms disrupt the in-plane symmetry, shifting the metal *d*-band center downward. This downward shift moderately weakens NO adsorption, preventing site poisoning, and significantly reduces the reaction overpotential. Systems like MnN_4O-C, FeN_4O-C, CoN_4O-C, and CoN_4F-C achieved remarkably low U_L (as low as −0.05 to −0.07 V) while effectively suppressing the competing HER. Collectively, these studies demonstrate that coordination microenvironment engineering, through manipulating in-plane coordination numbers, second-sphere interactions, and axial ligands, is a multi-faceted strategy for the rational design of highly active and selective NORR catalysts.

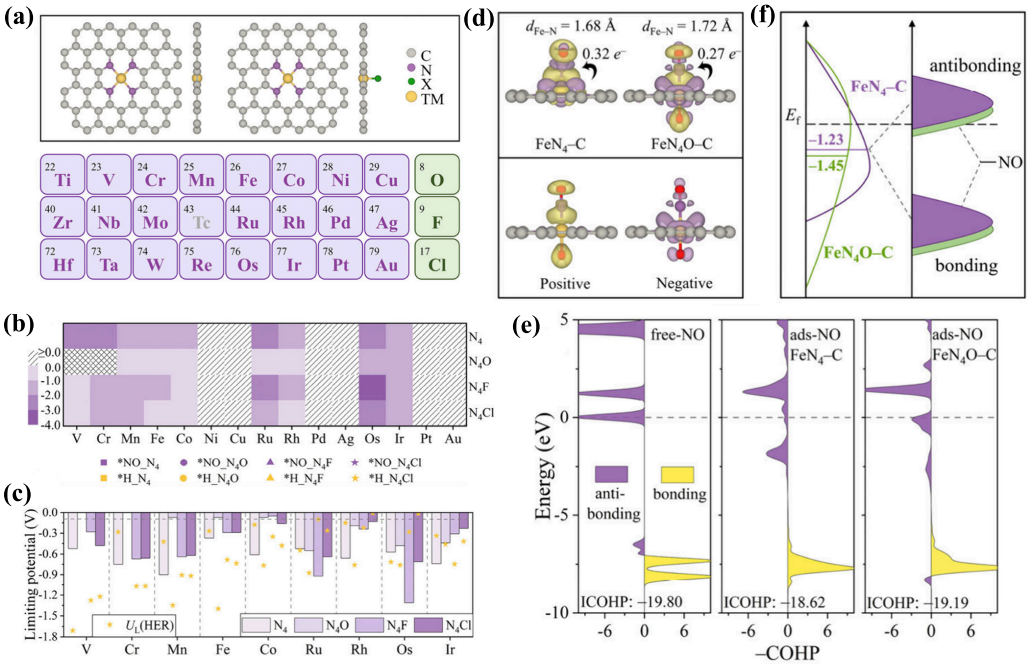


Figure 3. (**a**) Top and side views of TMN_4-C and TMN_4X-C structures. Metal and X atoms of consideration. (**b**) ΔG_{*NO} values for the 60 candidates. Grid shading indicates that NO cannot be stably adsorbed in any configuration, or the optimized configuration undergoes huge change. Slash shading suggests NO adsorption with positive adsorption free energy. (**c**) NORR limiting potential (U_L) on the 34 TMN_4-C and TMN_4X-C SACs, with the HER U_L shown for comparison. (**d**) Charge density difference for NO adsorption on FeN_4-C and FeN_4O-C SACs, charge transfer quantities are denoted. (**e**) COHP and ICOHP for free and adsorbed NO on FeN_4-C and FeN_4O-C SACs. (**f**) Schematics for the Fe *d*-band centers of FeN_4-C and FeN_4O-C SACs and the Fe-NO bonding antibonding states. Reproduced from Ref. [45] with permission from the American Chemical Society.

3.4. Doping Engineering

Doping with heteroatoms is a well-established method to modulate the electronic structure of materials, and it has gained renewed research attention in NORR catalyst design. By introducing foreign atoms into a host lattice, it is possible to optimize the

electronic properties of active centers and even create new ones. Recent theoretical studies have systematically explored this strategy across various 2D materials, demonstrating that single metal atom doping not only enhances NO adsorption and activation but also enables precise control over reaction pathways and product selectivity. For instance, doping 2D MA_2Z_4 materials with transition metals such as Cr, Zr, or Pt significantly lowers the limiting potential for NO-to-NH_3 conversion, with $Cr_1@HfSi_2N_4$ achieving an exceptionally low value of 0.11 V via the associative alternating-O pathway [46]. Similarly, TM-doped $MoSi_2N_4$ monolayers, particularly Zr- and Pt-doped systems, exhibit near-zero U_L and high selectivity against competing HER [47]. Beyond activity, the steric environment around dopants, exemplified by Fe-doped defective MoS_2, can steer the reaction away from byproduct formation (e.g., N_2O) by leveraging local alloying and spatial confinement [48]. Moreover, tuning the coordination environment of Cu in WX_2 (X = S, Se, Te) monolayers reveals that chalcogen identity modulates the *d*-band center and charge transfer, directly impacting the PDS [20].

Beyond metal doping, non-metal doping has also proven effective. Nie et al. [49] constructed metal-free NORR catalysts by doping C or O into h-BN. They discovered that C-doped h-BN can efficiently adsorb and activate NO, achieving a low limiting potential of −0.28 V while effectively suppressing HER, demonstrating the potential of metal-free systems. These diverse examples highlight doping engineering as a versatile strategy to modulate reaction pathways and intermediate adsorption behavior.

3.5. Strain Engineering

Applying mechanical strain is an elegant physical approach to continuously tune the electronic structure and, consequently, the catalytic activity of 2D materials. Sun et al. [50] investigated the effect of biaxial tensile strain on the β-$PdBi_2$ monolayer. As the strain increased from 0% to 7%, the NO adsorption strength gradually weakened. The PDS remained the first hydrogenation (*NO to *NHO), but its free energy change decreased significantly from 0.35 eV to 0.09 eV, greatly enhancing NORR activity. COHP analysis revealed that increased strain raises the occupancy of Bi-N antibonding states, thereby weakening adsorption in a classic example of Sabatier optimization. Sa and co-workers [51] systematically studied MoB_2 and WB_2 monolayers under biaxial strains ranging from −2% to 2%. They observed that increasing strain shifts the *p*/*d*-band center toward the Fermi level, optimizing the adsorption energies of intermediates. The WB_2 monolayer achieved optimal NORR activity at a moderate 1% tensile strain, with a limiting potential as low as −0.08 V. The observed volcanic relationship between strain and activity confirms that a balanced approach is necessary to optimize the trade-off between NO activation and NH_3 desorption. These studies collectively establish strain engineering as a powerful tool for fine-tuning NORR performance through continuous electronic structure modulation.

3.6. Heterojunction Engineering

Constructing van der Waals heterojunctions provides another dimension for catalyst design, as the interface between two distinct materials can give rise to unique electronic properties and abundant active sites. Zhou et al. [52] pioneered this concept in NORR by constructing an h-BN/graphene heterojunction and introducing a metal-free C center (CN_2 moiety) at the interface, achieving efficient NO activation with a limiting potential of −0.22 V. Yao et al. [53] adopted a different approach by supporting graphene on transition metal substrates like Ni and Co (Figure 4). They utilized a thermodynamic self-regulation effect to “pull” single metal atoms away from the substrate, forming unique dv-g/TM structures. Upon NO adsorption, a kinetic self-regulation induces a dynamic evolution

of the Ni single atom's coordination environment, effectively breaking the limitations of adsorption energy scaling relationships. Guo et al. [54] focused on MXene/graphene heterojunctions and discovered that B atom doping at the interface serves a dual role: it acts as an active center and as an electron transport bridge, significantly enhancing interfacial charge transfer and NO activation. Systems like B@$Mo_2ZrC_2O_2$-v/G were found to enable spontaneous NORR, confirming the unique regulatory role of *p*-block elements in such heterojunctions. In addition, Wen and colleagues [55] introduced a twist angle into metal-intercalated BN-graphene heterojunctions. They found that the twist angle modulates the orbital coupling strength between the metal and the active site, directing electron transfer to the BN surface and optimizing the electronic structure of the B site. By combining these findings with machine learning, they established a quantitative descriptor linking the twist angle to catalytic activity. These studies reveal the profound links between interface structure, electronic modulation, and NORR performance, propelling the field towards multi-degree-of-freedom synergistic catalyst design.

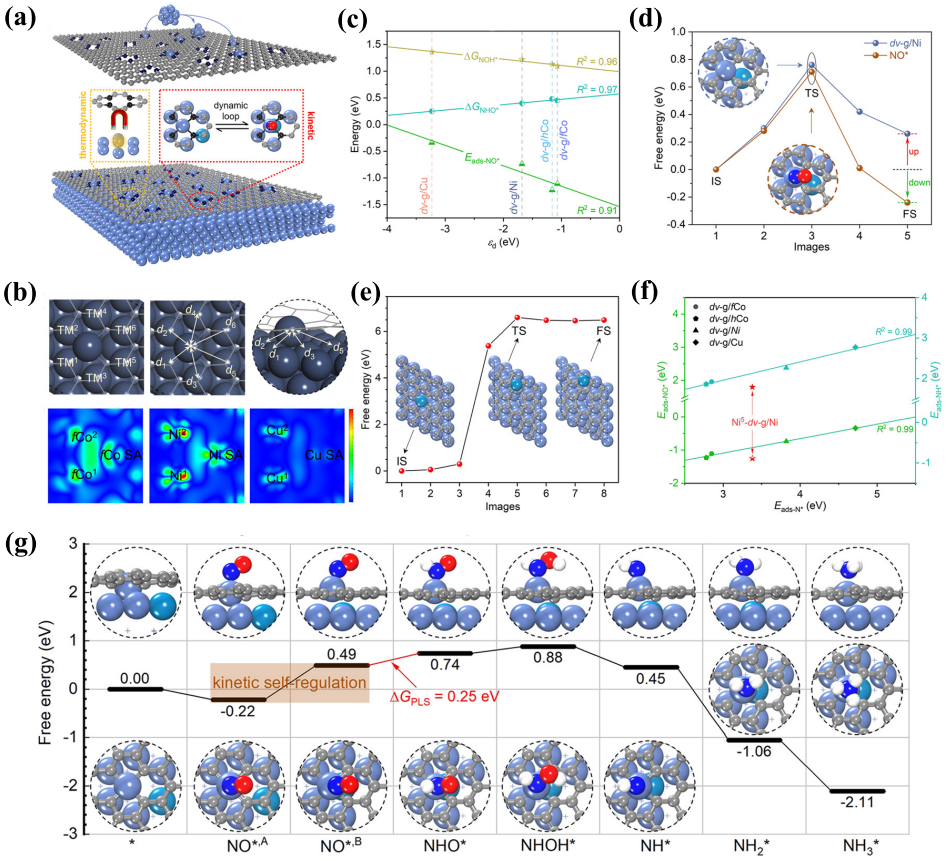


Figure 4. Schematic illustrations of (**a**) low capture efficiency of defects on SAs in general SACs and 100% capture efficiency of divacancies on SAs in g/TM due to thermodynamic self-regulation, involving the dynamic loop related to the adsorbate-assisted and reversible vacancy migration. (**b**) Schematic illustrations of TM^0 to TM^6 and d_1 to d_6. 2D charge density difference plots for dv-g/Co, dv-g/Ni, and dv-g/Cu plotted from 0 (blue) to 0.03 e/Å^3 (red). (**c**) $E_{ads\text{-}ON^*}$, ΔG_{NHO^*}, and ΔG_{NOH^*} as the functions of ε_d for dv-g/TM. (**d**) Kinetic energy barriers of Ni vacancy migration to the Ni^5 atom in free dv-g/Ni and NO* adsorbed dv-g/Ni. (**e**) Kinetic energy barrier of the diffusion of Ni SAs in dv-g/Ni, where IS, TS, and FS denote the initial state, transition state, and final state, respectively. (**f**) Relations between $E_{ads\text{-}NO^*}$ and $E_{ads\text{-}N^*}$, $E_{ads\text{-}NH^*}$ and $E_{ads\text{-}N^*}$ for dv-g/TM, including the points of Ni^5-dv-g/Ni. (**g**) Charge variations of Ni SAs in Ni@g, dv-g/Ni, and Ni^5-dv-g/Ni compared with the corresponding free catalysts (*), including the Bader charge values of Ni SAs. Reproduced from Ref. [53] with permission from the American Chemical Society.

Beyond the choice of active-site composition, the crystallographic orientation and surface structure of catalysts play crucial roles in NORR performance. Different crystal facets expose distinct atomic arrangements and electronic structures, leading to varying adsorption strengths and reaction pathways. For example, Cu(111) and Cu(100) surfaces exhibit markedly different NO adsorption energies and hydrogenation barriers, reflecting the influence of surface atomic density and coordination number [56]. Surface reconstruction—the rearrangement of surface atoms under reaction conditions—can also dramatically alter catalytic properties. In situ characterization studies have revealed that many transition metal surfaces undergo reconstruction in the presence of adsorbed NO or under applied potential, forming new surface phases with distinct catalytic behavior. Furthermore, crystal phase effects are particularly relevant for materials such as MoS_2, where the 1T (metallic) and 2H (semiconducting) phases exhibit dramatically different catalytic activities for NORR [57]. These crystallographic considerations underscore the importance of controlling synthesis conditions to achieve the desired surface structure and phase for optimal NORR performance.

Having surveyed various active-site engineering strategies, we now provide a side-by-side comparison of representative catalysts in Table 1, which compiles key performance indicators—limiting potential, selectivity, stability evidence, and the underlying design strategy—to facilitate cross-class evaluation.

Table 1. Summary of representative NORR catalysts with key performance metrics.

Catalyst Type	Representative Systems	Limiting Potential (V)	Selectivity	Stability	Main Design Strategy
Metal–N_4	Fe–N_4 [32], Co–N_4 [58]	−0.58 to −0.26	HER suppression	AIMD, E_b vs. E_{coh}	Coordination environment engineering
MXene-supported	Cu@$Ti_3C_2O_2$ [34]	Spontaneous	N_2O suppression	CPMD at 300–600 K	Vacancy anchoring
h-BN supported	Pd@B_2N_2 [59]	−0.55	HER/ammoxidation suppressed	E_b vs. E_{coh}	Single-atom embedding
DACs	Cr_2@C_2N [40], Mo_2@g-CN [39]	−0.05 to −0.43	N_2O/N_2 suppression	AIMD	Synergistic metal–metal interaction
2D materials	β-$PdBi_2$ [50], Cu_2Si [60]	−0.35 to spontaneous	HER suppression	E_b vs. E_{coh}, AIMD, U_{diss}	Strain engineering, topological properties
Metal-free	C-doped h-BN [49], 2P@C_2N [61]	−0.28 to 0	HER/N_2O suppression	AIMD	Non-metal doping

4. New Mechanisms in NORR Catalysis

While traditional transition metal-based catalysts have been extensively studied, their performance is often constrained by the scaling relations inherent to the d-band model. Recently, researchers have begun to explore deeper regulatory mechanisms that leverage the intrinsic degrees of freedom of electronic states, spin ordering, and surface reactivity. These novel strategies, including p-block element synergy, reverse activation, magnetic and spin modulation, and the exploitation of surface electronic singularities, offer pathways to transcend conventional limitations and open new avenues for designing highly active and selective NORR catalysts.

4.1. p-Block Element Synergy

The catalytic role of main-group p-block elements, traditionally considered inert, is being increasingly recognized. Liu et al. [62] systematically studied Group IIIA main-group metals (Al, Ga, and In) anchored on defective C_3N under four distinct coordination environments. Their work revealed that tetracoordinated structures exhibit significantly higher catalytic activity than their tricoordinated counterparts. A linear relationship between the Bader charge of the main-group metal and the reaction energy barrier was established, identifying charge transfer capability as the intrinsic origin of the activity differences. Wang et al. [63] anchored main-group metals (Mg, Ca, Al, Ga, In, Ge, Sn, Sb, and Bi) onto a BC_3 monolayer with monovacancy and found that Al@V_B, Ga@V_B, and Ge@V_C possess both thermodynamic stability and the ability to drive a spontaneous NORR process with negative ΔG_{max}, challenging the transition metal-centric design paradigm. Ren and colleagues, through first-principles calculations, evaluated the potential of a 2D Cu_2Si monolayer, a topological nodal-line semimetal, as a NORR catalyst [60]. They discovered that the *p*-block element Si plays a crucial role. Compared to a pure Cu(111) surface, the introduction of Si atoms significantly weakens NO adsorption and activates the NO molecule through a unique "donation/back-donation" mechanism. COHP analysis and charge density difference maps showed strong hybridization between the Si *3p* orbital and the NO *2p* orbital, enabling bidirectional charge transfer. This synergy not only effectively activates the N-O bond but also optimizes the adsorption energy of key intermediates, offering a general strategy to overcome scaling relations.

4.2. Reverse Activation Mechanism

The fully occupied surface orbitals of many 2D semiconductors are generally believed to render their basal planes inert, whereas conventional catalysts rely on active sites to activate reactants. In reverse activation, however, the reactant (NO) first induces electronic rearrangement on the catalyst surface, which then activates the reactant, following a "substrate-activates-catalyst-activates-substrate" sequence. Zang and co-workers, through their study of a series of 2D materials like CrX and Cr_2PY, proposed the novel concept of quasi-inert electrocatalysts [64]. As shown in Figure 5, despite the surface P/As atoms possessing fully occupied sp^3 hybrids, these materials exhibit excellent chemisorption and catalytic activity towards polar NO molecules. The phenomenon is attributed to a reverse activation mechanism. In this scenario, the polar adsorbate (NO), with its half-filled π^* orbital and asymmetric electron cloud distribution, first triggers an electronic rearrangement on the inert surface. This is followed by a multi-step electronic process involving charge transfer, donation, and back-donation, ultimately leading to the activation of NO. This discovery provides a new perspective for inert surface catalysis, revealing a mode where the adsorbate itself activates the substrate, and offers a theoretical basis for designing highly selective catalysts for polar small molecules like NO and CO.

4.3. Magnetism and Spin Regulation

Magnetism, an intrinsic property of many transition metal-based materials, is increasingly recognized as a powerful handle for controlling catalytic processes. The spin state of electrons in magnetic catalysts is a key electronic degree of freedom. By regulating magnetic ordering (e.g., switching between ferromagnetic and antiferromagnetic states), the intermediate binding strength of catalysts can be precisely modulated, offering an effective handle for catalytic performance tuning. Wang et al. [65] used a graphene-supported one-dimensional ferromagnetic Co chain as a model system to investigate the evolution of the catalyst's magnetic state during NORR. They found that the magnetic ground state is highly sensitive to adsorbates, applied potential, and pH. As the NORR reaction pro-

ceeds, the catalyst's magnetic state undergoes multiple transitions, directly affecting the adsorption configuration and binding strength of key intermediates, thereby altering the free energy profile. This study reveals a profound link between magnetic phase transitions and catalytic activity. Ma and colleagues [66] explored the possibility of breaking linear scaling relationships through magnetic state modulation in a 2D $Cr_2TiC_2T_2$ MXene system. They discovered that switching the magnetic order from antiferromagnetic to ferromagnetic significantly enhanced catalytic activity, with U_L dropping dramatically (e.g., from -0.77 V to -0.14 V for $Cr_2TiC_2F_2$). The microscopic origin lies in the magnetic state change shifting the *d*-band center of the active Cr atom upward, selectively stabilizing the key $*NH_3$ intermediate and making the otherwise endothermic $*NH_2 \rightarrow *NH_3$ step facile. Zhang et al. [67] applied spin engineering to SAC design, systematically investigating the effects of doping heteroatoms (e.g., B, N, F, Si, P, S, Cl) on the electronic structure and NORR activity of a single Fe center anchored on Ti_2CO_2 MXene. The dopants, through *p*-*d* orbital hybridization, effectively reconstructed the charge distribution, orbital energy levels, and spin-polarized state of the Fe center. Cl doping, for instance, enabled optimal matching between the Fe d orbitals and the NO $2\pi^*$ orbital, achieving efficient NO activation with a limiting potential as low as -0.36 V. This work not only identified a high-performance catalyst but also proposed an orbital-based activity descriptor, providing a new theoretical tool for designing high-spin NORR catalysts.

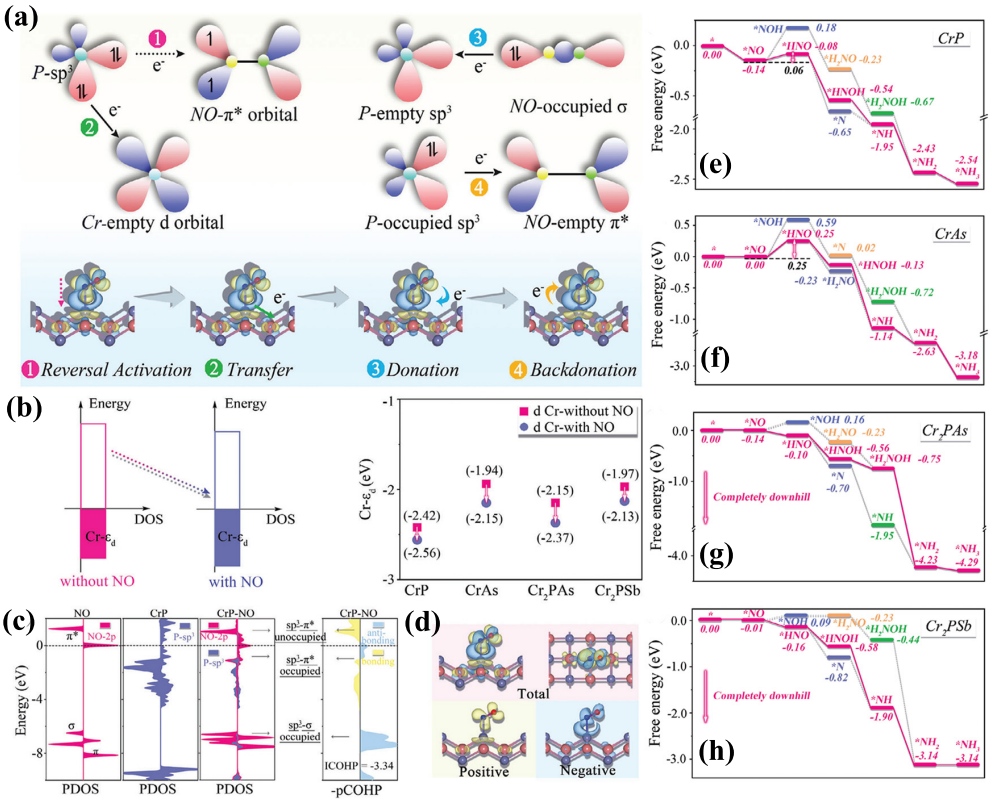


Figure 5. (**a**) Schematic illustration of the proposed Reversal Activation–Transfer–Donation/Backdonation mechanism. (**b**) Calculated Cr-*d* band centers (ε_d) on monolayer CrP, CrAs, Cr_2PAs, and Cr_2PSb before and after NO adsorption. (**c**) Projected density of states (PDOS) for a free NO molecule, the pristine CrP monolayer, and the NO-adsorbed CrP system, along with the corresponding projected crystal orbital Hamilton population (−pCOHP) for the P–NO interaction in the adsorbed state. (**d**) Charge density difference plots for NO adsorbed on monolayer CrP. Gibbs free energy diagrams for NORR on monolayer (**e**) CrP, (**f**) CrAs, (**g**) Cr_2PAs, and (**h**) Cr_2PSb via different pathways; the pink lines indicate the most favorable pathway. Reproduced from Ref. [64] with permission from the Wiley-VCH GmbH.

4.4. Surface Electronic Singularity

The intrinsic electronic structure of a material itself can be a source of exceptional catalytic activity. These are regions on the catalyst surface where the density of electronic states is unusually high, creating highly reactive "hot spots" for catalysis. Xiang et al. [68], using a particle-swarm optimization structure search method, predicted two novel 2D transition metal carbides, α-FeC_4 and β-FeC_4. These materials possess intrinsic metallic conductivity and, importantly, exhibit pronounced surface van Hove singularities near the Fermi level. These singularities, arising from flat bands in the electronic structure, lead to a sharp increase in the density of states, effectively creating a highly reactive electron reservoir. A strong linear correlation was found between the intensity of the surface van Hove singularity and the NO adsorption energy. By partially substituting Fe with Cu to create α-$CuFeC_4$, they further confirmed the localized nature of this effect, with NO preferentially adsorbing onto Fe atoms possessing stronger singularity characteristics. This study introduces the concept of surface van Hove singularities from condensed matter physics into the design of NORR catalysts, opening a new paradigm for exploring efficient catalysts based on novel electronic structures.

Beyond reporting individual catalyst performance, the rational design of NORR catalysts hinges on universal activity descriptors. To this end, Table 2 collates the key descriptors recently proposed in theoretical works, together with their applicable systems, correlation coefficients, and underlying physical interpretations, offering a concise reference for descriptor selection.

Table 2. Comparison of activity descriptors for NORR.

Descriptor	System	Correlation (R^2)	Physical Meaning
ΔG_{ads}(*N)	TM–N_4 [32]	0.90	N binding strength
ΔG_{ads}(*NO)	TM_2@C_2N [40], TMN_4X–C [45]	0.87–0.98	NO activation ability
d-band center (ε_d)	Fe SACs [43]	0.85	Metal–adsorbate interaction
ICOHP	TM–N_4 [32]	Linear	Bond strength

5. Reaction Microenvironment and Multifactor-Coupled Theoretical Simulations

Before delving into microenvironmental simulations, it is instructive to consider how theoretical predictions can be experimentally verified. Table 3 summarizes the principal in-situ and operando characterization techniques that enable real-time monitoring of catalyst structure, surface adsorbates, and reaction intermediates under operating conditions, thereby providing critical feedback for refining theoretical models. Beyond these tools, rigorous theory–experiment comparison requires precise control and measurement of pH, NO concentration, electrode potential, and solvation environment. Each factor is adjustable in the lab: pH is set by buffer solutions (phosphate for neutral, H_2SO_4 for acidic, KOH for alkaline) and monitored with microelectrodes or fluorescence probes; NO concentration is tuned by feed gas partial pressure or saturated electrolyte, with surface concentration quantified by RRDE or in situ DEMS; potential is applied by a potentiostat (typically -1.0 to 0.4 V vs. RHE) with IR compensation, and solvation is varied by solvent/co-solvent changes, probed by in situ SEIRAS or SFG spectroscopy. These experimentally controllable parameters not only enable rigorous validation of theoretical models but also define the boundary conditions that any realistic simulation must reproduce. Consequently, incorporating such multifaceted microenvironmental effects into theoretical frameworks has become a critical frontier in NORR research.

Table 3. Summary of in situ/operando characterization techniques for NORR catalyst studies.

Technique	Application	Information Obtained	Key Advantages	Limitations
In situ X-ray Absorption Spectroscopy (XAS)	Active-site structure under reaction conditions	Coordination environment, oxidation state, local geometry of metal centers	Element-specific; can be performed under actual operating conditions (potential, electrolyte)	Requires synchrotron radiation; ensemble-averaged information
Environmental Transmission Electron Microscopy (ETEM)	Morphology evolution under gas/liquid environments	Particle size distribution, agglomeration, surface reconstruction, structural degradation	Direct visualization at atomic scale; real-time monitoring	Electron beam damage; challenges with liquid-phase imaging
Surface-Enhanced Infrared Absorption Spectroscopy (SEIRAS)	Surface species identification during reaction	Adsorbed intermediates (*NO, *NHO, *NOH, etc.), adsorption configurations, reaction pathways	High surface sensitivity; distinguishes different adsorption configurations	Requires plasmonic substrates (Au, Ag); limited to certain frequency ranges
Differential Electrochemical Mass Spectrometry (DEMS)	Real-time product detection during electrolysis	Identification and quantification of volatile products (NH_3, N_2O, N_2, H_2)	Real-time, quantitative; distinguishes products from reactants	Only detects volatile species; complex calibration required
Rotating Ring-Disk Electrode (RRDE)	Mechanistic studies and intermediate detection	Detection of reaction intermediates, product selectivity, reaction kinetics	Quantitative; distinguishes between different reaction pathways	Limited to soluble species; requires careful electrode preparation
In situ Raman Spectroscopy	Surface species and catalyst structure	Adsorbed species, catalyst phase changes, surface reconstruction	High chemical specificity; can be performed in aqueous environments	Fluorescence interference; relatively low sensitivity
In situ X-ray Diffraction (XRD)	Crystal structure under operating conditions	Phase identification, lattice parameter changes, facet orientation, structural stability	Direct structural information; can track phase transitions	Limited surface sensitivity; requires crystalline samples
In situ Photoelectron Spectroscopy (XPS/UPS)	Surface chemical states under reaction conditions	Surface composition, chemical states, electronic structure	Surface-sensitive; provides direct chemical state information	Requires UHV or near-ambient pressure conditions

For instance, the surface coverage (θ) of reactants or intermediates can drastically reshape reaction landscapes. Its impact is dual-faceted: it can exacerbate side reactions or, conversely, induce beneficial self-promotion. AIMD simulations on $Cr_2@C_2N$ illustrate that sequential NH_3 generation occurs at low NO coverage (θ_{NO}). However, at high θ_{NO}, adjacent NO molecules readily couple into $*N_2O_2$ dimers, shifting selectivity toward N_2O. Similarly, on $TM@BC_3N_2$ catalysts, high NO concentrations promote N_2 byproduct formation [40]. In contrast, Mo_2C nanosheets exhibit coverage-induced self-promotion under operating bias, forming a dense *NH adsorption layer [69]. This layer not only facilitates the rapid reduction of free NO via N-N coupling but also creates a "HER-insulating shield" through electrostatic repulsion, raising the energy barrier for H^+ approach to over 2 eV and thereby synergistically enhancing both NORR activity and selectivity. Structural steric hindrance offers another avenue to suppress side reactions beyond dynamic coverage effects. Confined cavities, such as sulfur vacancies in MoS_2 [70] or antisite defects in $1T'$-MoX_2 [71], physically preclude N-N coupling by restricting the spatial proximity required for dimer formation, thus ensuring high NH_3 selectivity. Despite these advances, quantitative models linking coverage to catalytic activity and selectivity remain underdeveloped, and capturing the dynamic evolution of coverage under operando conditions continues to challenge current in situ characterization capabilities.

Meanwhile, theoretical methods are evolving to better capture electrochemical reality. The classical CHE model assumes fixed potential and charge neutrality, meaning it inadequately represents true electrochemical interfaces. More sophisticated approaches are increasingly bridging this gap, including constant potential methods, grand canonical density functional theory, and explicit solvation models. For example, constant potential

method calculations on NiB [72] and Mn-COF [7] show that interfacial electric field gradients significantly stabilize polar intermediates, yielding lower overpotential predictions than those obtained with the CHE model. This underscores the importance of capturing the nonlinear relationship between applied potential and intermediate adsorption energies.

Solvation effects add further complexity, as hydrogen-bond networks within explicit water models can fundamentally alter NORR pathways and the PDS. For instance, in the Cu-BHT metal–organic framework, hydrogen-bonding stabilization energies are sufficient to redefine the entire free energy landscape [73]. Local pH further modulates reaction selectivity. As shown in Figure 6, studies on FeN_4-C SACs reveal that NORR selectivity emerges from competition between the *HNO pathway (yielding NH_3) and the *ONNO pathway (yielding N_2O), governed synergistically by electrode potential, pH, and NO concentration [74]. Enhanced acidity, lower NO concentration, and more negative potentials favor NH_3 formation. Conversely, alkaline conditions, high NO concentration, and moderate potentials promote N-N coupling. These findings have enabled the construction of pH-potential phase diagrams for selectivity, offering quantitative theoretical guidance for experimental design. Although multifactorial simulations incorporating these elements are becoming more prevalent, their computational cost remains prohibitive for high-throughput screening, and the accuracy gap between simplified explicit models and true physical reality demands continued methodological refinement.

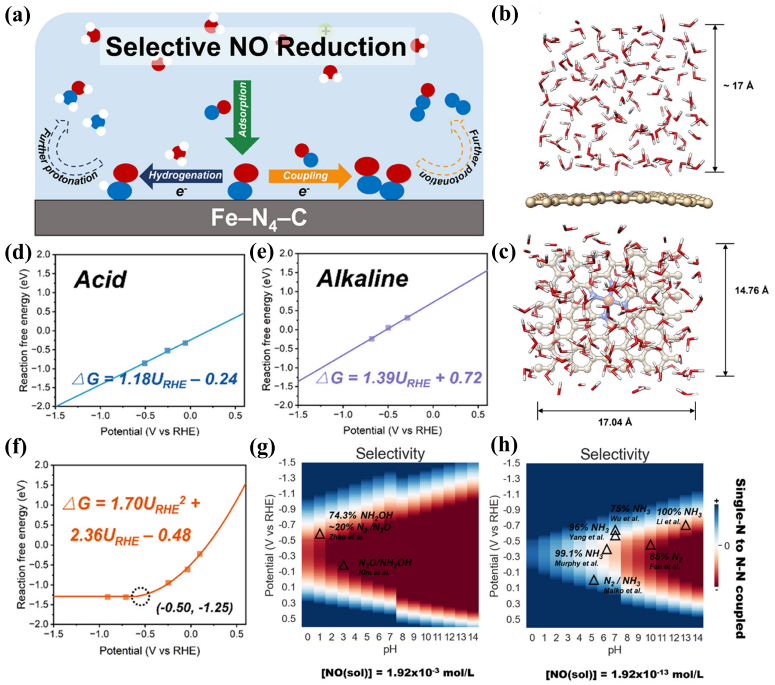


Figure 6. (**a**) Schematic representation of selective NORR pathways on a FeN_4-C catalyst model (N, O, and H atoms are colored blue, red, and white, respectively). Side view (**b**) and top view (**c**) of the FeN_4-C slab model embedded in a full explicit solvent environment at the potential of zero charge (PZC). Atoms are colored: C (ginger), N (blue), Fe (orange), O (red), H (white). Fitted linear relationships ($\Delta G - U$) for *HNO formation under (**d**) acidic and (**e**) alkaline conditions. (**f**) Fitted quadratic relationship ($\Delta G - U$) for *ONNO formation. Selectivity heat maps expressed as the equilibrium concentration ratio of key intermediates across a wide pH–potential space at NO concentrations of (**g**) 1.92×10^{-3} mol/L and (**h**) 1.92×10^{-13} mol/L. Reproduced from Ref. [74].

It is important to recognize that the majority of the catalytic performance predictions discussed in this review are derived from low-coverage, static DFT calculations employing the CHE model. While these predictions successfully capture qualitative trends and identify promising active sites, their quantitative accuracy is inherently constrained by the underde-

veloped linkage between surface coverage and selectivity. The overpotentials and Faradaic efficiencies cited should therefore be interpreted as semi-quantitative indicators of catalyst promise rather than as precise forecasts of experimental outcomes. The primary contribution of these theoretical screenings lies in identifying electronic and structural descriptors to guide experimental efforts, instead of pursuing absolute accuracy for practical device performance.

6. Machine Learning Accelerating Catalyst Screening

With the rapid expansion of the accessible materials space, data-driven methods such as machine learning are reshaping the discovery of electrocatalytic materials. Machine learning not only extracts structure–activity relationships from high-throughput data but also offers the potential to bypass linear scaling relations based on single adsorption energies. For instance, Kong et al. [75] combined DFT calculations with gradient boosting regression to study 26 transition metal SACs supported on phosphorene/carbon (TM-PCs), identifying the *d*-orbital vacancy rate of the transition metal as a key descriptor for NORR activity. Their machine learning analysis revealed that d-orbital-related features account for over 76% of the contribution. Furthermore, a volcano relationship exists between the d-orbital vacancy rate and the limiting potential. Guided by this descriptor, they identified Pt-PC as the optimal catalyst, achieving an exceptional U_L of −0.04 V. Similarly, Liu et al. [76] integrated grand canonical DFT calculations with extreme gradient boosting regression (XGBR) and sure independence screening and sparsifying operator (SISSO) to systematically screen Ag-based single-atom alloys (SAAs) for NO electroreduction to NH_3 (Figure 7). Their ML framework broke through the limitations of conventional linear scaling relations of intermediate adsorption free energies, pinpointing that the s-orbital density of states of dopant atoms near the Fermi level dominates NH_3 selectivity, while the average NO-metal bond length, first ionization energy, and d-band center of the dopant collectively govern catalytic activity quantified by the $\Phi_{max}(\eta)$ descriptor. This data-driven strategy successfully screened out Cu/Ag and Zn/Ag SAAs as high-performance candidates with suppressed hydrogen evolution and excellent activity–selectivity balance, and the SISSO-derived analytical formula enabled reliable and interpretable prediction of catalytic performance. These studies collectively demonstrate that machine learning not only accelerates screening but also uncovers physically meaningful "super descriptors," offering new perspectives for rational catalyst design.

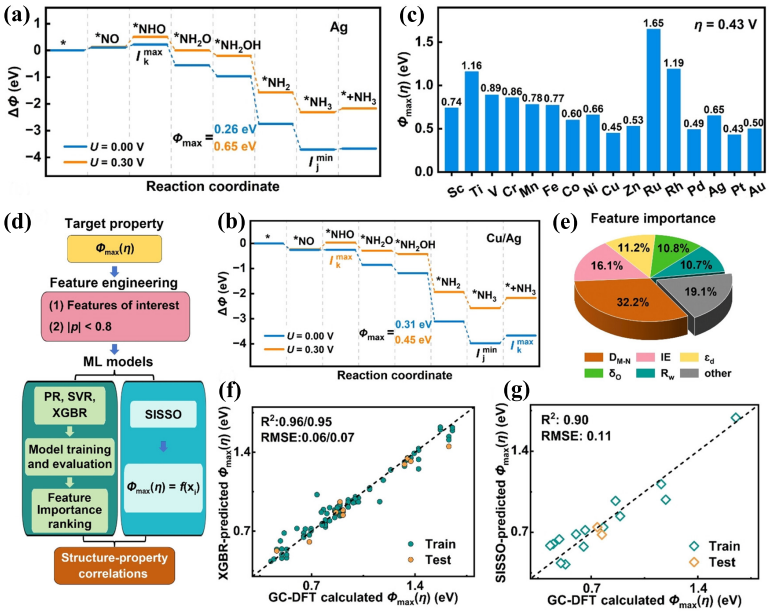


Figure 7. Grand free energy diagrams of (**a**) Ag, and (**b**) Cu/Ag at $U = 0$ V and 0.3 V vs. RHE. (**c**) The $\Phi_{max}(\eta)$ values for the SAAs catalysts. (**d**) Machine learning workflow with feature engineering.

(**e**) Comparison between GC-DFT and ML predicted $\Phi_{max}(\eta = 0.43$ V vs. RHE). (**f**) The ranking of the important features of XGBR. (**g**) Comparison between GC-DFT and SISSO predicted $\Phi_{max}(\eta = 0.43$ V vs. RHE). Reproduced from Ref. [76] with permission from the Wiley-VCH GmbH.

Despite its promise, several critical limitations must be acknowledged. First, the training datasets for ML models in NORR catalysis are typically small (often <100 data points), which limits the model's generalization capability and increases the risk of overfitting. Second, the DFT data used for training often come from inconsistent computational protocols—different exchange–correlation functionals, solvation models, and convergence criteria—which introduces systematic errors that ML models cannot easily correct. Third, descriptor transferability remains a major challenge: descriptors optimized for one class of catalysts (e.g., SACs) often fail when applied to another class (e.g., DACs or 2D materials). Fourth, and most importantly, there is a critical lack of experimental validation. Most ML predictions rely solely on DFT-calculated targets without experimental benchmarking, which makes it difficult to assess their true predictive power for real-world catalysis.

7. Conclusions and Perspectives

This review systematically summarizes recent theoretical advances in low-dimensional NORR electrocatalysts, focusing on five key aspects: reaction mechanisms, active-site engineering, electronic structure regulation, microenvironment effects, and machine learning applications. Current research has identified several promising strategies for catalyst design: optimizing intermediate adsorption energies through coordination environment engineering; broadening electronic structure tunability via doping, strain, and heterojunction construction; transcending scaling relations through emerging mechanisms such as p-block synergy, magnetic modulation, and reverse activation; and employing multi-factor coupled simulations that incorporate coverage, solvation, pH, and applied potential to bridge theory and experiment.

7.1. Catalyst Stability and Synthesis Challenges

Despite the proliferation of theoretically predicted high-activity catalysts, several critical challenges impede their translation into practical applications. Catalyst stability under operating conditions is among the most pressing issues. Theoretically optimized non-noble metal single-atom sites and defect-rich structures are prone to dissolution, agglomeration, or reconstruction in strong electric fields and electrolyte environments, leading to activity degradation. For SACs in particular, the high surface free energy of isolated metal atoms drives migration and aggregation into nanoparticles during wet-chemical synthesis or high-temperature pyrolysis—a phenomenon well documented in studies of Cu and Ni atoms on $Ti_3C_2O_2$ MXene supports. Even after successful preparation, active centers may undergo gradual leaching or Ostwald ripening upon prolonged electrolysis, especially under harsh pH or high-overpotential conditions.

Strategies to address these challenges include strengthening metal-support interactions, utilizing spatial confinement in porous matrices (e.g., zeolites, MOFs, and carbon defects), and applying protective overlayers. Future theoretical studies should incorporate energetic and kinetic descriptors of atom mobility and dissolution—such as diffusion barriers and dissolution potentials (U_{diss})—to guide the synthesis of stable, high-density single-atom sites. Equally important is the need for operando characterization—particularly X-ray absorption spectroscopy and environmental transmission electron microscopy—to track the dynamic evolution of active centers under realistic reaction conditions, thereby establishing reliable structure–activity–stability relationships.

7.2. Methodological Challenges and Multi-Fidelity Frameworks

Beyond stability, the computational methodology underpinning catalyst discovery requires fundamental upgrades. Data-driven catalyst screening still predominantly relies on static DFT calculations, which oversimplify reaction kinetics, solvent fluctuations, and potential-dependent charge redistribution. To provide a more reliable foundation for inverse catalyst design, cross-scale computational databases integrating grand canonical ensemble corrections, molecular dynamics trajectories, and experimental benchmarks are urgently needed. However, a critical challenge remains: reconciling the high accuracy of sophisticated microkinetic and solvation models with the high throughput required for screening. Multi-fidelity approaches offer a practical solution. In such a framework, cheap but physically meaningful descriptors (e.g., static DFT adsorption energies) are first used to filter a large materials space. For the reduced candidate set, medium-level corrections such as implicit solvation and constant-potential calculations are then applied. Only the top-ranked systems subsequently undergo high-fidelity evaluation using fully explicit solvation, grand canonical electronic structure methods, and ab initio molecular dynamics. To further enhance efficiency, machine learning surrogate models trained on the high-fidelity data can interpolate across chemical space. Meanwhile, Δ-machine learning corrects low-cost predictions toward higher accuracy. These strategies hold great promise for balancing computational expense and predictive power in future NORR catalyst discovery.

7.3. Transferability to Bulk and Three-Dimensional Architectures

The design principles distilled from low-dimensional models—local coordination engineering, strain effects, and heterojunction concepts—are not confined to 2D materials. Although this review concentrates on low-dimensional systems, many of these principles are transferable to bulk and three-dimensional catalyst architectures that are more relevant for industrial electrolyzers. Local coordination engineering, for instance, can be realized on high-surface-area carbons, metal oxides, and zeolites by creating isolated metal sites or bimetallic ensembles that mimic the electronic structure of 2D model catalysts. Strain effects, elegantly tuned in 2D monolayers through biaxial tension, can be induced in nanoparticles via core-shell architectures or support-induced lattice mismatch. Heterojunction concepts can be replicated by designing three-dimensional composite electrodes with well-defined interfacial contacts—for example, by coating 2D materials onto porous metal foams or by creating graded interfaces between different catalyst layers. Translating these strategies to scalable, three-dimensional architectures while preserving the precise active-site structures identified in low-dimensional models is a crucial step toward application at higher Technology Readiness Levels (TRL). This translation will require close collaboration between theorists, experimentalists, and chemical engineers to address challenges in mass transport, catalyst loading, and long-term operation.

7.4. Future Research Directions

Based on the challenges identified above, several specific research directions merit prioritization: (1) Coverage-dependent selectivity modeling: Quantitative models linking surface coverage to catalytic activity and selectivity remain underdeveloped. Future work should integrate operando experiments (e.g., in situ Raman, SEIRAS) with advanced simulations (e.g., grand canonical DFT, kinetic Monte Carlo) to capture the dynamic evolution of surface species under reaction conditions. (2) pH-dependent reaction mechanisms: The mechanistic origins of pH-dependent activity and selectivity are not fully understood. Constant-potential simulations coupled with explicit solvation models should be systematically applied to map the free energy landscapes of NORR across the full pH range (0–14), guiding experimental electrolyte design. (3) Accelerated catalyst discovery via

integrated ML-DFT workflows: Machine learning models for NORR currently suffer from small datasets and inconsistent DFT protocols. Future efforts should focus on building standardized, open-access databases of NORR intermediates, developing transferable descriptors that work across catalyst classes, and validating ML predictions with experimental measurements. (4) Stability predictions through long-timescale simulations: AIMD simulations typically span only tens of picoseconds, insufficient to capture degradation processes such as Ostwald ripening or surface reconstruction. Future methodological developments should aim for microsecond-scale simulations using machine learning potentials or accelerated molecular dynamics methods to predict catalyst lifetimes. (5) Bridging the gap to industrial electrolyzers: Most theoretical studies focus on idealized catalyst surfaces under low-coverage conditions. Future work should incorporate high-surface-coverage effects, mass transport limitations, and realistic electrode geometries to provide actionable guidance for membrane electrode assembly design and large-scale NORR implementation.

Author Contributions: Conceptualization, Y.L., D.Z. and H.Y.; methodology, W.W., S.X. and J.W.; software, W.W. and S.X.; validation, Y.L., D.Z. and H.Y.; formal analysis, Y.L. and H.Y.; resources, W.W., S.X. and J.W.; data curation, Y.L. and D.Z.; writing—original draft preparation, Y.L. and D.Z.; writing—review and editing, W.W. and J.W.; visualization, S.X.; supervision, H.Y. and J.W.; project administration, H.Y. and J.W.; funding acquisition, W.W. and S.X. All authors have read and agreed to the published version of the manuscript.

Funding: This work was supported by the Fundamental Research Funds for the Central Universities (No. WK9990000152).

Institutional Review Board Statement: Not applicable.

Informed Consent Statement: Not applicable.

Data Availability Statement: No new data were created or analyzed in this study. Data sharing is not applicable to this article.

Acknowledgments: The authors would like to thank the anonymous reviewers for their constructive comments.

Conflicts of Interest: The authors declare no conflicts of interest.

Abbreviations

The following abbreviations are used in this manuscript:

NORR	Electrocatalytic Nitric Oxide Reduction Reaction
NH_3	Ammonia
NO	Nitric Oxide
HER	Hydrogen Evolution Reaction
SAC	Single-Atom Catalyst
DAC	Dual-Atom Catalyst
2D	Two-Dimensional
TMD	Transition Metal Dichalcogenide
DFT	Density Functional Theory
PDS	Potential-Determining Step
U_L	Limiting Potential
CHE	Computational Hydrogen Electrode
AIMD	Ab Initio Molecular Dynamics
COHP	Crystal Orbital Hamilton Population
PDOS	Projected Density of States

References

1. Wu, Q.; Zhu, F.; Wallace, G.; Yao, X.; Chen, J. Electrocatalysis of nitrogen pollution: Transforming nitrogen waste into high-value chemicals. *Chem. Soc. Rev.* **2024**, *53*, 557–565. [CrossRef] [PubMed]
2. Xiong, S.; Wang, W.; Wang, F.; Li, S.; Liu, Y.; Zhuo, Z.; Zhang, Y.; Shen, X. Thermal catalytic synthesis of ammonia using uranium/graphdiyne composite at mild conditions. *Nat. Commun.* **2026**, *17*, 2894. [CrossRef] [PubMed]
3. Wang, D.; Chen, Z.-W.; Gu, K.; Chen, C.; Liu, Y.; Wei, X.; Singh, C.V.; Wang, S. Hexagonal Cobalt Nanosheets for High-Performance Electrocatalytic NO Reduction to NH_3. *J. Am. Chem. Soc.* **2023**, *145*, 6899–6904. [CrossRef] [PubMed]
4. Chen, K.; Xiang, J.; Guo, Y.; Liu, X.; Li, X.; Chu, K. Pd1Cu Single-Atom Alloys for High-Current-Density and Durable NO-to-NH_3 Electroreduction. *Nano Lett.* **2024**, *24*, 541–548. [CrossRef] [PubMed]
5. Shao, J.; Jing, H.; Wei, P.; Fu, X.; Pang, L.; Song, Y.; Ye, K.; Li, M.; Jiang, L.; Ma, J.; et al. Electrochemical synthesis of ammonia from nitric oxide using a copper–tin alloy catalyst. *Nat. Energy* **2023**, *8*, 1273–1283. [CrossRef]
6. Zhao, R.; Ma, Z.; Yu, Y.; Xia, X.; Song, B.; Zhou, T.; Huang, Y. Theoretical investigation on NO reduction electro-catalyzed by transition-metal-anchored SnOSe nanotubes. *Nano Res.* **2023**, *16*, 8533–8541. [CrossRef]
7. Yu, J.; Wang, Y.; Li, Y. A two-dimensional covalent organic framework with single-atom manganese for electrochemical NO reduction: A computational study. *Phys. Chem. Chem. Phys.* **2024**, *26*, 15120–15124. [CrossRef] [PubMed]
8. Chen, K.; Zhang, Y.; Xiang, J.; Zhao, X.; Li, X.; Chu, K. p-Block Antimony Single-Atom Catalysts for Nitric Oxide Electroreduction to Ammonia. *ACS Energy Lett.* **2023**, *8*, 1281–1288. [CrossRef]
9. Wang, H.; Ma, Y.; Bai, J.; Gu, Z.; Lai, K. Transition Metal-Embedded C_4N_4 Octahedral Rings as Highly Efficient Electrocatalysts for NO to NH_3 Conversion: A Computational Study. *Langmuir* **2025**, *41*, 31243–31252. [CrossRef] [PubMed]
10. Niu, H.; Liu, J.; Liu, Y.; Zhao, J. Unraveling the electronic origin of high activity and selectivity of single-atom catalysts for NO electroreduction. *New J. Chem.* **2026**, *50*, 136–144. [CrossRef]
11. Zang, Y.; Wu, Q.; Wang, S.; Huang, B.; Dai, Y.; Ma, Y. Coupling a Main-Group Metal with a Transition Metal to Create Biatom Catalysts for Nitric Oxide Reduction. *Phys. Rev. Appl.* **2023**, *19*, 024003. [CrossRef]
12. Lu, M.; Hu, T.; Kan, E. Tunable ferroelectric diatomic catalysis on In_2Se_3 monolayers for NO reduction. *J. Mater. Chem. A* **2025**, *13*, 41321–41332. [CrossRef]
13. Wang, D.; Zhu, X.; Tu, X.; Zhang, X.; Chen, C.; Wei, X.; Li, Y.; Wang, S. Oxygen-Bridged Copper–Iron Atomic Pair as Dual-Metal Active Sites for Boosting Electrocatalytic NO Reduction. *Adv. Mater.* **2023**, *35*, 2304646. [CrossRef]
14. Zhu, X.; Yuan, X.; Wang, Y.; Ge, M.; Tang, Y. Revealing the origin of activity in phthalocyanine-based dual-metal sites towards electrochemical nitric oxide reduction. *Chem. Commun.* **2023**, *59*, 9960–9963. [CrossRef]
15. Yan, Y.; Masood, Z.; Wang, B. Lanthanum-Doped Graphene for Electrocatalytic Reduction of Nitrogen Monoxide. *J. Phys. Chem. C* **2023**, *127*, 12967–12975. [CrossRef]
16. Li, Y.; Zheng, G.; Li, L.; Zhang, X.; Tian, Z.; Chen, L. Theoretical investigation of single-atom catalysts anchored on pure carbon substrate for electroreduction of NO to NH_3. *Phys. Chem. Chem. Phys.* **2022**, *24*, 29112–29119. [CrossRef] [PubMed]
17. Gao, Y.; Wang, E.; Zhou, J.; Sun, Z. Theoretical investigation of graphdiyne-supported single-cluster catalysts for electroreduction of nitric oxide. *Appl. Surf. Sci.* **2025**, *681*, 161522. [CrossRef]
18. Yan, T.; Wang, S.; Lang, S.; Wang, Z.; Lin, S.; Zhao, J. Screened Ni_3 single-cluster catalyst supported on graphidyne for high-performance electrocatalytic NO reduction to NH_3: A computational study. *J. Colloid Interface Sci.* **2025**, *683*, 1067–1076. [CrossRef] [PubMed]
19. Lin, L.; Pang, D.; Shi, P.; Xie, K.; Su, L.; Zhang, Z. First-principles study of TM supported $SnSe_2$ monolayer as an efficient electrocatalyst for NOER. *Mol. Catal.* **2022**, *533*, 112789. [CrossRef]
20. Jacob, R.; Padmanaban, R. Unveiling the Catalytic Activity and Selectivity by Tuning the Coordination Environment of Cu Embedded on the WX_2 (X = S, Se, and Te) Monolayer for the Nitric Oxide Reduction Reaction: Insights from the DFT Approach. *Langmuir* **2025**, *41*, 29346–29357. [CrossRef] [PubMed]
21. Liu, Y.; Tursun, M.; Hu, G.; Abdukayum, A.; Wu, C. Non-metal single atoms anchored on defective MoS_2: A novel electrocatalyst for NO reduction to NH_3. *RSC Adv.* **2025**, *15*, 29323–29334. [CrossRef] [PubMed]
22. Xu, Y.; He, C.; Zhao, C.; Fu, L. Single-atom Ti doping on S-vacancy two-dimensional CrS_2 as a catalyst for ammonia synthesis: A DFT study. *Chin. Chem. Lett.* **2025**, *36*, 109797. [CrossRef]
23. Jacob, R.; Doulassiramane, T.; Padmanaban, R. Highly-selective Electrocatalytic Reduction of NO to NH_3 using Cu Embedded WS_2 Monolayer as Single-atom Catalyst: A DFT Study. *ChemPhysChem* **2024**, *25*, e202400473. [CrossRef] [PubMed]
24. Liu, L.; Zhao, Y.; Lin, X.; Ren, C.; Gao, Y.; Zhu, W. Ammonia Synthesis via Nitric Oxide Electrochemical Reduction on OH-MXenes: A Universal Descriptor. *J. Phys. Chem. C* **2025**, *129*, 4067–4076. [CrossRef]
25. Zhao, S.; Li, Y.; Guo, Z.; Tang, C.; Sa, B.; Miao, N.; Zhou, J.; Sun, Z. Breaking scaling relations in nitric oxide reduction by surface functionalization of MXenes. *J. Mater. Chem. A* **2022**, *10*, 25201–25211. [CrossRef]
26. Huang, B.; Wu, Y.; Zhang, Z.; Chen, R.; Ren, G.; Zhou, N.; Li, N.; Qian, Y. Assembly of an actinide-uranium single atom catalyst on defective MXenes for efficient NO electroreduction. *J. Mater. Chem. A* **2025**, *13*, 16970–16980. [CrossRef]

27. Wang, D.; Lu, X.F.; Luan, D.; Lou, X.W. Selective Electrocatalytic Conversion of Nitric Oxide to High Value-Added Chemicals. *Adv. Mater.* **2024**, *36*, 2312645. [CrossRef]
28. Yang, Y.; Sun, C.; Zhuo, Z.; Wang, L.; Wang, W.; Lu, A.; Wang, J. Main-Group p-Block Metal-Doped C3N Monolayers as Efficient Electrocatalysts for NO-to-NH_3 Conversion: A Computational Study. *Langmuir* **2025**, *41*, 9011–9018. [CrossRef] [PubMed]
29. Jiang, H.; Rezaeimotlagh, A.; Nazari, S.; Zhou, R.; Li, T.; Huang, J.; Esrafilzadeh, D.; Jalili, A.R. A roadmap for ammonia synthesis via electrocatalytic reduction of nitric oxide. *Energy Environ. Sci.* **2025**, *18*, 9373–9422. [CrossRef]
30. Qiao, B.; Wang, A.; Yang, X.; Allard, L.F.; Jiang, Z.; Cui, Y.; Liu, J.; Li, J.; Zhang, T. Single-atom catalysis of CO oxidation using Pt_1/FeO_x. *Nat. Chem.* **2011**, *3*, 634–641. [CrossRef] [PubMed]
31. Zhang, L.; Yang, X.; Lin, J.; Li, X.; Liu, X.; Qiao, B.; Wang, A.; Zhang, T. On the Coordination Environment of Single-Atom Catalysts. *Acc. Chem. Res.* **2025**, *58*, 1878–1892. [CrossRef] [PubMed]
32. Wang, J.; Li, K.; Hao, Q.; Liu, D.; Zhang, X. Electroreduction NO to NH_3 over single metal atom anchored on pyrrole type defective graphene: A DFT study. *Chin. Chem. Lett.* **2023**, *34*, 107567. [CrossRef]
33. Duan, Y.; Wu, D.; Qin, Z. Tuning single metal atoms anchored on VS_2 for the electrochemical reduction of nitric oxide to ammonia: A computational study. *Electrochim. Acta* **2025**, *538*, 146954. [CrossRef]
34. Kong, L.; Wang, M.; Wu, C.-M.L. From Single Atom to Low-Nuclearity Cluster Immobilized Ti_3C_2TX MXene for Highly Efficient NO Electroreduction to NH_3. *ACS Mater. Lett.* **2024**, *6*, 1711–1721. [CrossRef]
35. Zhang, M.; Cao, X.; Dong, J.; Zhu, X.; Zhu, Y.; Wang, L. Unveiling the Mystery of Precision Catalysis: Dual-Atom Catalysts Stealing the Spotlight. *Small* **2025**, *21*, 2409560. [CrossRef]
36. Wang, J.; Yi, G.; Guo, S.; Wang, J.; Li, S.; Xu, K.; Wang, W.; Lei, S. Computational design of bimetallic TM_2@g-C_9N_4 electrocatalysts for enhanced CO reduction toward C_2 products. *Chin. Chem. Lett.* **2024**, *35*, 109050. [CrossRef]
37. Wang, J.; Shi, M.; Yi, G.; Wang, L.; Lei, S.; Xu, K.; Li, S.; Mu, J. Computational prediction of Mo_2@g-C_6N_6 monolayer as an efficient electrocatalyst for N_2 reduction. *Chin. Chem. Lett.* **2022**, *33*, 4623–4627. [CrossRef]
38. Zhou, P.; Ruan, W.; Zhou, T.; Guan, J. Advancements in dual-atom-site catalysts for electrocatalysis. *Nano Res.* **2026**, *19*, 94907996. [CrossRef]
39. Sun, X.; Dai, Y.; Huang, B.; Wei, W. High-Throughput Screening of Effective Dual Atom Catalysts for the Nitric Oxide Reduction Reaction. *J. Phys. Chem. Lett.* **2023**, *14*, 11684–11690. [CrossRef] [PubMed]
40. Zang, Y.; Wu, Q.; Wang, S.; Huang, B.; Dai, Y.; Ma, Y. High-Throughput Screening of Efficient Biatom Catalysts Based on Monolayer Carbon Nitride for the Nitric Oxide Reduction Reaction. *J. Phys. Chem. Lett.* **2022**, *13*, 527–535. [CrossRef] [PubMed]
41. Fan, J.; Yang, L.; Sun, Z.; Li, H.; Ye, L.; Mei, M.; Zhu, W. Heteronuclear double transition metal synergistic regulation of nitric oxide electroreduction reaction. *Int. J. Hydrogen Energy* **2025**, *185*, 151983. [CrossRef]
42. Zhao, Y.; Lu, B.; An, Z.; Wang, H.; Li, X. Insight into the mechanism on NO reduction over dual-atom Fe-Cu catalyst supported on N-dopped graphene: A DFT study. *Appl. Surf. Sci.* **2025**, *682*, 161769. [CrossRef]
43. Li, H.; Wu, D.; Wu, J.; Lv, W.; Duan, Z.; Ma, D. Graphene-based iron single-atom catalysts for electrocatalytic nitric oxide reduction: A first-principles study. *Nanoscale* **2024**, *16*, 7058–7067. [CrossRef] [PubMed]
44. Zhu, X.; Song, X.; Yang, W.; Yu, C.; Qiu, J. Modifying the second coordination spheres of Fe active sites for electrocatalytic nitric oxide reduction in realistic electrochemical environment. *Appl. Surf. Sci.* **2024**, *678*, 161129. [CrossRef]
45. Sun, Y.; Huang, B.; Dai, Y.; Wei, W. Improving Nitric Oxide Reduction Reaction Activity of TMN_4-C Model Catalysts by Axial Atom Coordination. *J. Phys. Chem. Lett.* **2025**, *16*, 9–16. [CrossRef] [PubMed]
46. Sun, X.; Zheng, J.; Yao, Z.; Deng, S.; Pan, Z.; Wang, S.; Wang, J. DFT Investigation of Single Metal Atom-Doped 2D MA_2Z_4 Materials for NO Electrocatalytic Reduction to NH_3. *J. Phys. Chem. C* **2022**, *126*, 17598–17607. [CrossRef]
47. Tong, T.; Linghu, Y.; Wu, G.; Wang, C.; Wu, C. Nitric oxide electrochemical reduction reaction on transition metal-doped $MoSi_2N_4$ monolayers. *Phys. Chem. Chem. Phys.* **2022**, *24*, 18943–18951. [CrossRef] [PubMed]
48. Yang, L.; Fan, J.; Zhu, W. Using ternary steric hindrance synergy of a defective MoS_2 monolayer to manipulate the electrocatalytic mechanism toward nitric oxide reduction: A first-principles and machine learning study. *J. Mater. Chem. A* **2023**, *11*, 7159–7169. [CrossRef]
49. Nie, J.; Li, Y.; Gao, D.; Fang, Y.; Lin, J.; Tang, C.; Guo, Z. Carbon doped hexagonal boron nitride as an efficient metal-free catalyst for NO capture and reduction. *Phys. Chem. Chem. Phys.* **2024**, *26*, 2539–2547. [CrossRef] [PubMed]
50. Sun, Y.; Wang, Z.; Liu, Y.; Cai, Q.; Zhao, J. The β-$PdBi_2$ monolayer for efficient electrocatalytic NO reduction to NH_3: A computational study. *Inorg. Chem. Front.* **2023**, *10*, 2677–2688. [CrossRef]
51. Sa, R.; Li, Q.; Li, W.; Wu, H.; Li, D.; Ma, Z.; Liu, D. Strain-engineered molybdenum Diboride and tungsten Diboride monolayers as efficient catalysts for sustainable ammonia production via nitric oxide reduction. *J. Colloid Interface Sci.* **2025**, *700*, 138597. [CrossRef] [PubMed]
52. Zhou, Q.; Gong, F.; Xie, Y.; Xia, D.; Hu, Z.; Wang, S.; Liu, L.; Xiao, R. A general strategy for designing metal-free catalysts for highly-efficient nitric oxide reduction to ammonia. *Fuel* **2022**, *310*, 122442. [CrossRef]

53. Yao, X.; Huang, L.; Halpren, E.; Chen, L.; Chen, Z.; Singh, C.V. Structural Self-Regulation-Promoted NO Electroreduction on Single Atoms. *J. Am. Chem. Soc.* **2023**, *145*, 26249–26256. [CrossRef] [PubMed]
54. Guo, F.; Ma, J.; Deng, X.; Gao, H. B modulating MXene/Graphene heterojunction catalyst for highly efficient NO electrochemical synthesis of ammonia. *Fuel* **2025**, *393*, 135055. [CrossRef]
55. Wen, X.; Prezhdo, O.V.; Xu, L. Design of Twisted Two-Dimensional Heterostructures and Performance Regulation Descriptor for Electrocatalytic Ammonia Production from Nitric Oxide. *J. Am. Chem. Soc.* **2025**, *147*, 14647–14658. [CrossRef] [PubMed]
56. Xiao, L.; Mou, S.; Dai, W.; Yang, W.; Cheng, Q.; Liu, S.; Dong, F. Identification of Cu(111) as Superior Active Sites for Electrocatalytic NO Reduction to NH_3 with High Single-Pass Conversion Efficiency. *Angew. Chem. Int. Ed.* **2024**, *63*, e202319135. [CrossRef]
57. Tursun, M.; Wu, C. NO Electroreduction by Transition Metal Dichalcogenides with Chalcogen Vacancies. *ChemElectroChem* **2021**, *8*, 3113–3122. [CrossRef]
58. Wang, Z.; Zhao, J.; Wang, J.; Cabrera, C.R.; Chen, Z. A Co-N_4 moiety embedded into graphene as an efficient single-atom-catalyst for NO electrochemical reduction: A computational study. *J. Mater. Chem. A* **2018**, *6*, 7547–7556. [CrossRef]
59. He, C.-Z.; Zhang, Y.-X.; Wang, J.; Fu, L. Anchor single atom in h-BN assist NO synthesis NH_3: A computational view. *Rare Met.* **2022**, *41*, 3456–3465. [CrossRef]
60. Ren, Z.; Zhang, H.; Wang, S.; Huang, B.; Dai, Y.; Wei, W. Nitric oxide reduction reaction for efficient ammonia synthesis on topological nodal-line semimetal Cu_2Si monolayer. *J. Mater. Chem. A* **2022**, *10*, 8568–8577. [CrossRef]
61. Wu, Q.; Wang, H.; Shen, S.; Huang, B.; Dai, Y.; Ma, Y. Efficient nitric oxide reduction to ammonia on a metal-free electrocatalyst. *J. Mater. Chem. A* **2021**, *9*, 5434–5441. [CrossRef]
62. Liu, S.; Xing, G.; Yu, H.; Liu, J.-Y. C_3N-supported IIIA group metal single-atom catalysts with different coordination microenvironments: Electrocatalytic NO reduction to ammonia. *Appl. Surf. Sci.* **2024**, *649*, 159130. [CrossRef]
63. Wang, J.; Sun, C.; Sheng, L.; Zhuo, Z.; Li, S.; Wang, J.; Wang, W.; Sun, J.; Yang, J.; Xu, K.; et al. Unveiling the electrocatalytic potential of main-group metal-embedded BC_3 monolayer for highly efficient NO reduction to NH_3. *Chin. Chem. Lett.* **2026**, *37*, 110974. [CrossRef]
64. Zang, Y.; Wu, Q.; Wang, S.; Huang, B.; Dai, Y.; Heine, T.; Ma, Y. Unveiling Pseudo-Inert Basal Plane for Electrocatalysis in 2D Semiconductors: Critical Role of Reversal-Activation Mechanism. *Adv. Energy Mater.* **2024**, *14*, 2303953. [CrossRef]
65. Wang, Z.-P.; Chen, Y.-J.; Fang, S.-Y.; Zhang, X.-J.; Zhang, W.; Sun, F.-L.; Chen, W.-X.; Zhuang, G.-L. Magnetic transition of 1D ferromagnetic catalysts during the NO electroreduction. *J. Catal.* **2024**, *434*, 115524. [CrossRef]
66. Ma, L.; Yang, Y.; Li, Y.; Yu, Y.; Gao, D.; Guo, Z.; Qi, Y.; Long, L.; Tang, C. Promoting the electrocatalytic nitric oxide reduction by modulating the magnetic states of MXene. *Appl. Surf. Sci. 2025*, *695*, 162878. [CrossRef]
67. Zhang, Y.; Su, K.; Huang, B. Heteroatom-doping-engineered spin state of single-atom Fe on MXene for electrocatalytic NO-to-NH_3 conversion. *Appl. Surf. Sci.* **2026**, *720*, 165264. [CrossRef]
68. Xiang, Y.; Wang, M.; Lin, Y.; Zhao, Y.; Wu, S.; Sun, Y.; Zhu, Z.-Z.; Cao, X. Theoretical Investigation of Two-Dimensional FeC_4 Structures with Surface Van Hove Singularity for Electrochemical Nitric Oxide Reduction Reaction. *J. Phys. Chem. Lett.* **2025**, *16*, 475–482. [CrossRef] [PubMed]
69. Huang, X.; Hu, X.; Wang, J.; Xu, H. Self-Promoting NO electrochemical reduction via N-N coupling by Surface-Adsorbed *NH intermediates on Mo_2C nanosheets. *J. Catal.* **2025**, *446*, 116097. [CrossRef]
70. He, B.; Lv, P.; Wu, D.; Li, X.; Zhu, R.; Chu, K.; Ma, D.; Jia, Y. Confinement catalysis of a single atomic vacancy assisted by aliovalent ion doping enabled efficient NO electroreduction to NH_3. *J. Mater. Chem. A* **2022**, *10*, 18690–18700. [CrossRef]
71. Tursun, M.; Wu, C. Defective 1T'-MoX_2 (X = S, Se, Te) monolayers for electrocatalytic ammonia synthesis: Steric and electronic effects on the catalytic activity. *Fuel* **2023**, *342*, 127779. [CrossRef]
72. Chen, W.; Xiang, Y.; Wu, Z.; Wang, M.; Fang, Y.; Zhu, Z.-Z.; Wu, S.; Cao, X. NiB monolayer: A topological metal with high NORR electrocatalytic perfomance. *Appl. Surf. Sci.* **2023**, *637*, 157887. [CrossRef]
73. Yin, H.; Gong, M.; Lyu, P.; Wang, R.; Sun, L. Theoretical Insights into the Selective Electrocatalytic Reduction of NO to NH_3 on a Two-Dimensional Cu-Benzylthiol Metal–Organic Framework Nanostructure. *ACS Appl. Nano Mater.* **2024**, *7*, 5180–5191. [CrossRef]
74. Qian, S.J.; Cao, H.; Wang, Y.G.; Li, J. Controlling the Selectivity of Electrocatalytic NO Reduction through pH and Potential Regulation on Single-Atom Catalysts. *J. Am. Chem. Soc.* **2024**, *146*, 12530–12537. [CrossRef] [PubMed]
75. Kong, L.; Liang, X.; Wang, M.; Wu, C.-M.L. Role of transition metal *d*-orbitals in single-atom catalysts for nitric oxide electroreduction to ammonia. *J. Colloid Interface Sci.* **2023**, *647*, 375–383. [CrossRef] [PubMed]
76. Liu, J.; Wang, S.; Tian, Y.; Guo, H.; Chen, X.; Lei, W.; Yu, Y.; Wang, C. Screening of Silver-Based Single-Atom Alloy Catalysts for NO Electroreduction to NH_3 by DFT Calculations and Machine Learning. *Angew. Chem. Int. Ed.* **2025**, *64*, e202414314. [CrossRef]

Disclaimer/Publisher's Note: The statements, opinions and data contained in all publications are solely those of the individual author(s) and contributor(s) and not of MDPI and/or the editor(s). MDPI and/or the editor(s) disclaim responsibility for any injury to people or property resulting from any ideas, methods, instructions or products referred to in the content.